Broadband and High-Gain Microstrip Patch Antenna Loaded With Parasitic Mushroom-Type Structure

Yufan Cao, Yang Cai, Wenquan Cao, Baokun Xi, Zuping Qian, Tao Wu, and Lei Zhu

***Abstract*—This letter presents a novel broadband microstrip patch antenna with a simple geometry. Two parasitic mushroom-type arrays are incorporated along with the two radiating edges of a main radiating patch. First, thanks to the mushroom-type structure, a new resonant mode, characterized as quasi-TM_{30} mode, is generated. Besides, the main radiating patch produces the original TM_{10} mode. Thus, wideband performance is realized on the basis of the two combined modes. Second, the current distributions on those metal patches are nearly uniform so that high gains are achieved over the entire operating bandwidth. Measured results indicate that the enhanced impedance bandwidth is from 11.9 to 18.2 GHz, which covers the whole Ku-band. Meanwhile, a nearly constant peak-radiating gain between 10 and 10.5 dBi at broadside radiation is obtained. The proposed antenna maintains the advantages of wide bandwidth, ease of fabrication, flat and high gains, and a low profile less than $\lambda_0/13$ thickness substrate.**

***Index Terms*—Broadband, high gain, microstrip patch antenna, mushroom-type structure.**

I. Introduction

MICROSTRIP patch antenna has been widely researched and employed in many devices due to its attractive advantages of low profile, ease of fabrication, conformability to a shaped surface, compatibility with integrated circuit technology, etc. [1]. With the development of 5G communication, the wideband and high-gain antennas are in great demand. However, the conventional microstrip antenna suffers from the drawback of narrow bandwidth, which restricts its applications in wireless communications.

A variety of methods were employed to broaden bandwidth of microstrip patch antennas, such as increasing substrate thickness [2], cutting slots inside the patch [3], employing aperture-coupled feeding network [4], building shorting walls [5], applying parasitic strips around the patch [6], using hybrid-coupling method [7], and stacking patches on multilayered substrate [8]. The aforementioned methods are effective for broadening the bandwidth of microstrip patch antennas, but they bring out new challenges in other aspects, such as size reduction, gain improvement, planar structure, and good radiation performances.

Recently, kinds of metamaterial-based antennas have been proposed to achieve wideband performance [9]. As one of the representative metamaterials, mushroom structures are widely applied in the design of broadband antennas. One of the basic applications of mushroom structure is mushroom antennas. A low-profile broadband mushroom antenna was presented in [10], and an impedance bandwidth of 25% was obtained because of dual resonance modes that were excited simultaneously. A low-profile low-temperature co-fired ceramic (LTCC)-based metamaterial-mushroom antenna array fed by substrate integrated waveguide (SIW) was proposed, and an impedance bandwidth from 56.3 to 65.7 GHz was attained [11]. Loading mushroom-type structure on the conventional antennas is another promising application. Combining meta-mushroom structure and a SIW cavity-backed slot antenna, a new broadband antenna with bandwidth from 4.5 to 5.6 GHz was designed [12]. Loading mushroom-like rectangular patches on the top of a planar slot antenna, a dual-band antenna was achieved for wireless local area network applications [13]. Through loading mushroom-type metamaterial at SIW horn aperture, a fractional impedance bandwidth of 10.6% was obtained on a $\lambda_0/20$ thickness substrate [14]. However, most of the aforementioned antennas are constructed on multilayered substrate.

On the basis of our previous work [15], mushroom-type structure is loaded along with the two radiating edges of a conventional patch on the same substrate, and a detailed mechanism analysis is presented in this letter. The conventional TM_{10} mode and a new quasi-TM_{30} mode are simultaneously excited, resulting in broad bandwidth.

II. Antenna Design

A. Antenna Geometry

The geometrical configuration of the proposed mushroom-loaded patch antenna is described in Fig. 1, which comprises three parts: a main radiating patch, two parasitic mushroom-type arrays symmetrically placed along with the two radiating edges of the main radiating patch, and a ground plane with size of $l_g \times w_g$. The main radiating patch occupies an area of $l \times w$. As for the mushroom-type structure, an array includes three

Manuscript received March 17, 2019; revised April 25, 2019; accepted May 15, 2019. Date of publication May 20, 2019; date of current version July 3, 2019. This work was supported in part by the National Natural Science Foundation of China under Grant 61271103 and in part by the Jiangsu Province Natural Science Foundation under Grant BK20160080. *(Corresponding author: Yang Cai.)*

Y. Cao, W. Cao, Z. Qian, and L. Zhu are with the College of Communications Engineering, Army Engineering University of PLA, Nanjing 210007, China (e-mail: caoyufan135@sina.com; cao_wenquan@163.com; qzp811@sina.com; zhulei_paper@126.com).

Y. Cai and T. Wu are with the Space Engineering University, Beijing 101400, China (e-mail: caiyang_1991@163.com; 15101100181@139.com).

B. Xi is with the Key Laboratory of High Power Microwave Sources and Technologies, Institute of Electronics, Chinese Academy of Sciences, Beijing 100190, China (e-mail: zqbxxbk@163.com).

Digital Object Identifier 10.1109/LAWP.2019.2917909

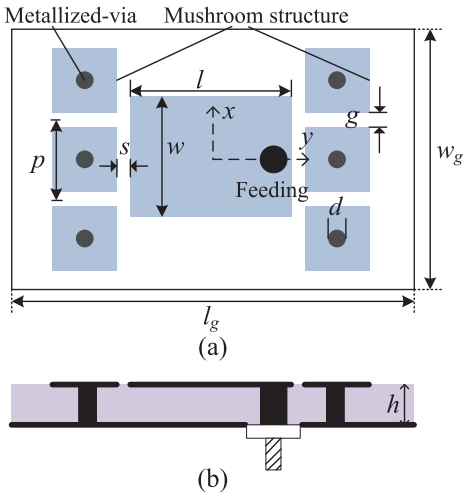

Fig. 1. Geometrical configuration of the proposed patch antenna. (a) Top view. (b) Side view.

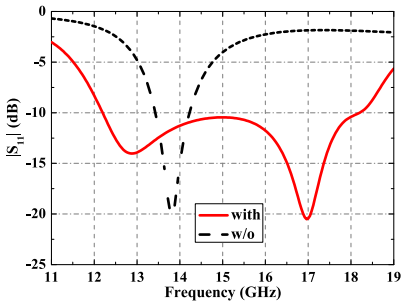

Fig. 2. Simulated $|S_{11}|$ of the patch antenna with and without the mushroom-type structure.

mushroom units, and all of the mushroom units are identical in size. One mushroom unit is composed of a square patch with periodicity p and a center-placed metallized via with diameter d. The gap between mushroom units is g, and the coupling gap between the main radiating patch and mushroom-type structure is s. This antenna is constructed on a substrate with permittivity of 2.2, loss tangent of 0.0009, and thickness of 1.524 mm, and coaxial feeding method is employed.

B. Comparison With Conventional Patch Antenna

A conventional patch antenna, with same size and feeding method as employed in the proposed antenna, is introduced for comparison. Since the mushroom-type structure is the unique difference, simulated $|S_{11}|$ of the patch antenna with and without the mushroom-type structure are compared in Fig. 2. A new resonant frequency is excited due to the loaded mushroom-type structure so that wide bandwidth from 12 to 18 GHz is achieved.

The electric field distributions at two resonant frequencies are studied in order to indicate the effectiveness of the loaded mushroom-type structure intuitively. The simulated current distribution and electric field distribution at resonant frequency

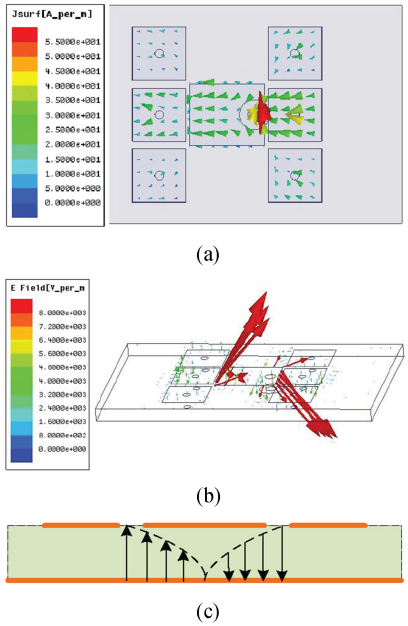

Fig. 3. TM_{10} mode at resonant frequency 12.89 GHz. (a) Simulated current distribution. (b) Simulated electric field distribution. (c) Sketch of the operation mechanism.

12.89 GHz are illustrated in Fig. 3. It is obvious that the electric field distribution is similar to the TM_{10} mode just like a conventional patch antenna. In fact, the main radiating patch in the proposed antenna plays an important part in radiating energy to free space at low operating frequencies. In this case, little energy is transmitted to the mushroom-type structure, so the effect of loaded mushroom-type structure can be neglected.

Fig. 4 depicts the simulated current distribution and electric field distribution at the new resonant frequency 17 GHz. It is found that the electric field distribution resembles the TM_{30} mode, namely quasi-TM_{30} mode. A part of energy is coupled to the mushroom-type structure through coupling gaps. Therefore, energy can be radiated to free space through two coupling gaps and two edges of mushroom-type structure.

In order to determine the resonant frequency for the quasi-TM_{30} mode in theory, a transmission-line model is employed to analyze the proposed patch antenna. Since the fringing field exists at the open edges of the mushroom-type structure, the extended length can be approximated to that of the corresponding entire rectangular patch, as given in [10]

$$\varepsilon_{\text{eff}} = \frac{\varepsilon_r + 1}{2} + \frac{\varepsilon_r - 1}{2}\left(1 + 12\frac{h}{W_p}\right)^{-\frac{1}{2}} \tag{1}$$

$$\Delta L = 0.412h\frac{(\varepsilon_{\text{eff}} + 0.3)\,(W_p/h + 0.262)}{(\varepsilon_{\text{eff}} - 0.258)\,(W_p/h + 0.813)} \tag{2}$$

$$W_p = Np - g \tag{3}$$

$$\beta_e = k_0\sqrt{\varepsilon_{\text{eff}}} = \frac{2\pi f}{c}\sqrt{\varepsilon_{\text{eff}}} \tag{4}$$

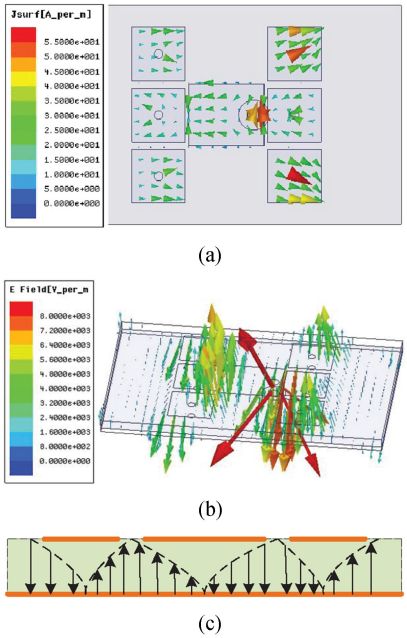

Fig. 4. Quasi-TM_{30} mode at resonant frequency 17 GHz. (a) Simulated current distribution. (b) Simulated electric field distribution. (c) Sketch of the operation mechanism.

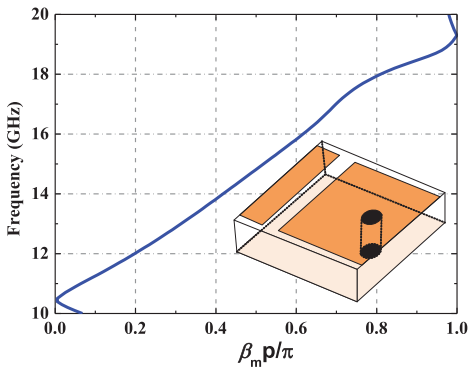

Fig. 5. Dispersion diagram of the mushroom unit.

where ε_{eff} denotes the effective dielectric constant of the substrate, ΔL the extended length, W_p the width of the mushroom-type structure, N the number of mushroom units, and N equals 3 in this letter. β_e represents the propagation constant in the extended region, k_0 the wavenumber in free space, f the operating frequency, and c the free-space velocity of light.

The propagation constant β_m of the mushroom unit can be derived from the simulated dispersion diagram, as depicted in Fig. 5. It is observed that the proposed patch antenna is operated in the right-handed region. The resonant frequency for the quasi-TM_{30} mode is approximatively calculated by

$$\beta_m pN/3 + 2\beta_e \Delta L = \pi. \tag{5}$$

All in all, the resonant frequency for the quasi-TM_{30} mode can be calculated through formula (5), which is 17.9 GHz (where

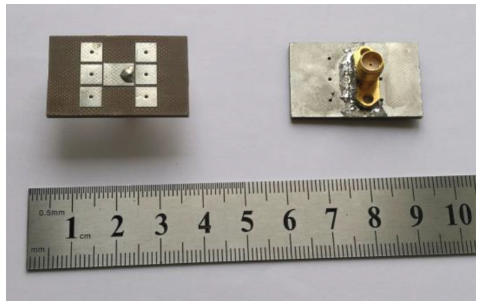

Fig. 6. Photograph of the proposed patch antenna.

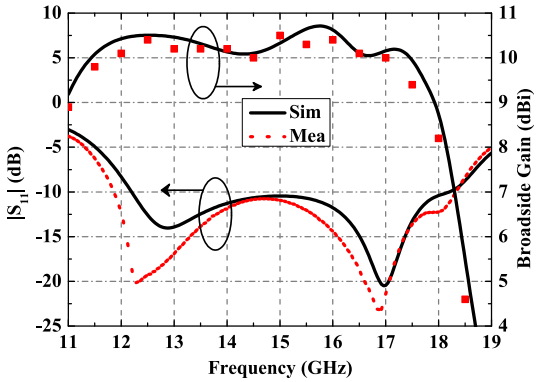

Fig. 7. Simulated and measured $|S_{11}|$ and broadside gains of the proposed antenna.

the corresponding $\beta_m p/\pi$ is 0.794). The calculated frequency for the quasi-TM_{30} mode is slightly shifted from the simulated one of 17 GHz because the main driven patch has an effect on the resonant frequency. What is more, in order to effectively excite quasi-TM_{30} mode, two requirements should be first satisfied; First, the number of mushroom units in one side should be odd, and second, the antenna structure should be symmetrical along the x-axis and y-axis.

For a conventional patch antenna, since the resonant frequency of the TM_{30} mode is about thrice that of the TM_{10} mode, it is impossible to realize wide bandwidth through combining TM_{10} mode and TM_{30} mode. However, by loading mushroom-type structure, the resonant frequency of the quasi-TM_{30} mode is close to that of the TM_{10} mode, resulting in wide impedance bandwidth.

III. Experimental Results

A prototype of the proposed antenna is designed and fabricated to validate the simulated results, as depicted in Fig. 6. By optimizing the geometry of the mushroom-type loaded patch antenna with the HFSS software, the optimized parameters are as follows: $w = 5.6$ mm, $l = 6.9$ mm, $l_g = 32$ mm, $w_g = 20$ mm, $s = 0.3$ mm, $g = 0.7$ mm, $p = 5.6$ mm, $d = 0.8$ mm, $h = 1.5$ mm. The commercial SMA connector is located along the y-axis, and offset distance is 2.5 mm. The simulated and measured reflection coefficients and broadside gains are illustrated in Fig. 7. The measured results show that the proposed patch

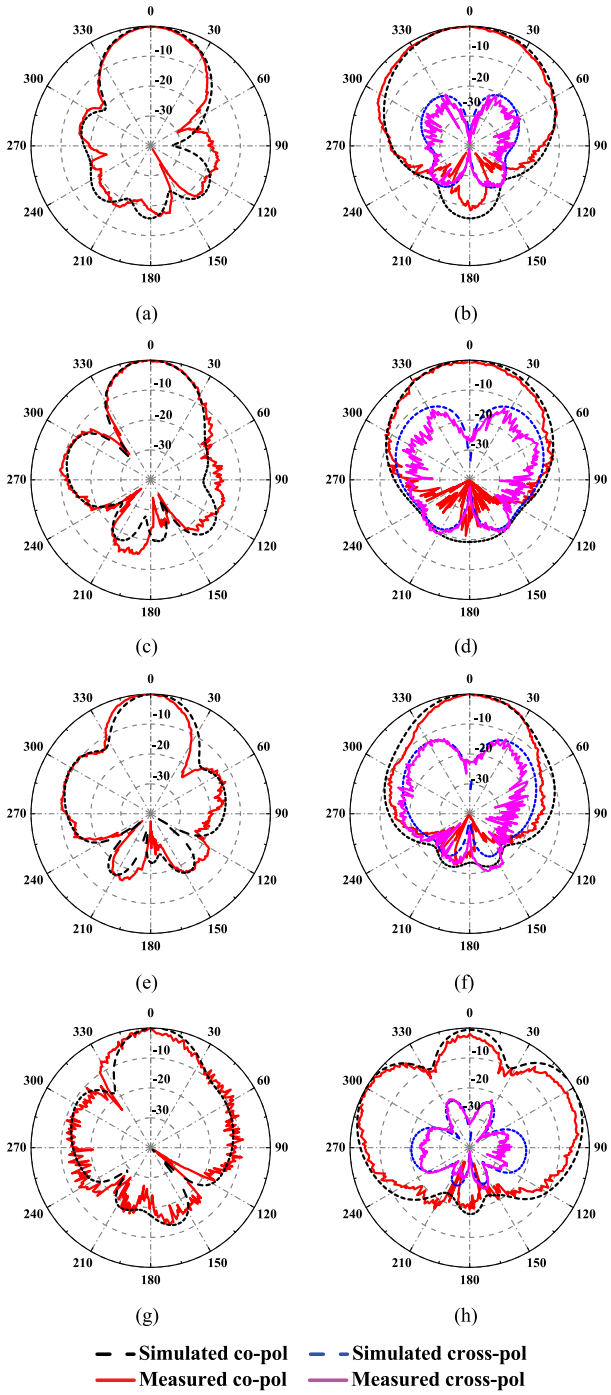

Fig. 8. Simulated and measured far-field radiation patterns of the proposed antenna at four representative frequencies. (a) E-plane at 12 GHz. (b) H-plane at 12 GHz. (c) E-plane at 14 GHz. (d) H-plane at 14 GHz. (e) E-plane at 16 GHz. (f) H-plane at 16 GHz. (g) E-plane at 18 GHz. (h) H-plane at 18 GHz.

antenna operates from 11.9 to 18.2 GHz with $|S_{11}|$ below -10 dB, which is more than 40% at the central frequency 15 GHz. The measured resonant frequencies are slightly shifted downwards to the lower frequency, which may come from the dielectric loss and fabrication tolerance. What is more, the measured gains indicate that a nearly constant peak-radiating gain between 10 and 10.5 dBi from 12 to 17 GHz at boresight direction is obtained. The superiority of flat high gains makes the proposed antenna available for broad applications.

TABLE I
COMPARISON WITH PREVIOUSLY PUBLISHED DESIGNS

Num.	Impedance Bandwidth	0.5-dB Gain Bandwidth	3-dB Gain Bandwidth	Thickness	Number of Layers
[8]	34.9%	about 8.1%	about 30%	$0.08\lambda_0$	3
[10]	25%	about 7.6%	about 29%	$0.075\lambda_0$	2
[12]	22%	about 10%	about 30%	$0.08\lambda_0$	3
[14]	10.6%	about 3.5%	about 13%	$0.05\lambda_0$	1
This work	40%	34.5%	46%	$0.075\lambda_0$	1

The simulated and measured far-field radiation patterns at four representative frequencies across the entire bandwidth are illustrated in Fig. 8. Good agreements are observed between the simulated results and the measured ones. Stable broadside radiation patterns for the proposed antenna are obtained. Besides, the cross-polarization level is less than -40 dB in the E-plane, so it does not appear in Fig. 8. The measured cross-polarization level is less than -25 dB in the H-plane. Moreover, the beamwidths in E-plane are narrower than that of conventional patch antenna, leading to high gains. At high frequencies of the operating bandwidth, the quasi-TM_{30} mode dominates, leading to the high side-lobe level (SLL), which can be observed from the radiation pattern at 18 GHz as shown in Fig. 8(h). The main radiation direction maintains broadside direction, but the gains are decreased rapidly because of the high SLL, which explains the sharply decreased gains after 18 GHz in Fig. 7.

IV. CONCLUSION

In this letter, a novel broadband and high-gain microstrip patch antenna is investigated. By employing mushroom-type structure along with two radiating edges of a main radiating patch, wide impedance bandwidth characteristic is achieved because of the newly generated quasi-TM_{30} mode. Measured results indicate that the enhanced impedance bandwidth of more than 40% covering the whole Ku-band is obtained. In addition, the proposed antenna exhibits stable broadside radiation patterns over the entire operating frequency with flat high gains around 10 dBi. The structural characteristics and the performance of the proposed antenna and other previous antennas are compared in Table I, which indicates that the proposed antenna owns the advantages of wide impedance bandwidth, high-gain flatness, low profile, and easy fabrication.

REFERENCES

[1] K. F. Lee and K. F. Tong, "Microstrip patch antennas—Basic characteristics and some recent advances," *Proc. IEEE*, vol. 100, no. 7, pp. 2169–2180, Jul. 2012.

[2] D. H. Schaubert, D. M. Pozar, and A. Adrian, "Effect of microstrip antenna substrate thickness and permittivity: Comparison of theories and experiment," *IEEE Trans. Antennas Propag.*, vol. 37, no. 6, pp. 677–682, Jun. 1989.

[3] A. A. Deshmukh and K. P. Ray, "Compact broadband slotted rectangular microstrip antenna," *IEEE Antennas Wireless Propag. Lett.*, vol. 8, pp. 1410–1413, 2009.

[4] Y. Jia, Y. Liu, and S. Gong, "Slot-coupled broadband patch antenna," *Electron. Lett.*, vol. 51, no. 6, pp. 445–447, Mar. 2015.

[5] Y. C. Chi, C. H. Chan, and K. M. Luk, "Study of a small wide-band patch antenna with double shorting walls," *IEEE Antennas Wireless Propag. Lett.*, vol. 3, pp. 230–231, 2004.

[6] S. H. Wi, Y. S. Lee, and J. G. Yook, "Wideband microstrip patch antenna with U-shaped parasitic elements," *IEEE Trans. Antennas Propag.*, vol. 55, no. 4, pp. 1196–1199, Apr. 2007.

[7] K. P. Ray, G. Kumar, and H. C. Lodwal, "Hybrid-coupled broadband triangular microstrip antennas," *IEEE Trans. Antennas Propag.*, vol. 51, no. 1, pp. 139–141, Jan. 2003.

[8] V. P. Sarin, M. S. Nishamol, D. Tony, C. K. Aanandan, P. Mohanan, and K. Vasudevan, "A wideband stacked offset microstrip antenna with improved gain and low cross polarization," *IEEE Trans. Antennas Propag.*, vol. 59, no. 4, pp. 1376–1379, Apr. 2011.

[9] Y. Dong and T. Itoh, "Metamaterial-based antennas," *Proc. IEEE*, vol. 100, no. 7, pp. 2271–2285, Jul. 2012.

[10] W. Liu, Z. N. Chen, and X. Qing, "Metamaterial-based low-profile broadband mushroom antenna," *IEEE Trans. Antennas Propag.*, vol. 62, no. 3, pp. 1165–1172, Mar. 2014.

[11] W. Liu, Z. N. Chen, and X. Qing, "60-GHz thin broadband high-gain LTCC metamaterial-mushroom antenna array," *IEEE Trans. Antennas Propag.*, vol. 62, no. 9, pp. 4592–4601, Sep. 2014.

[12] H. Kang and S. O. Park, "Mushroom metamaterial based substrate integrated waveguide cavity backed slot antenna with broadband and reduced back radiation," *Microw., Antennas Propag.*, vol. 10, no. 14, pp. 1598–1603, Nov. 2016.

[13] Z. Wu, L. Li, X. Chen, and K. Li, "Dual-band antenna integrating with rectangular mushroom-like superstrate for WLAN applications," *IEEE Antennas Wireless Propag. Lett.*, vol. 15, pp. 1004–1007, 2016.

[14] Y. Cai, Y. S. Zhang, L. Yang, Y. F. Cao, and Z. P. Qian, "Design of low-profile metamaterials-loaded substrate integrated waveguide horn antenna and its array applications," *IEEE Trans. Antennas Propag.*, vol. 65, no. 7, pp. 3732–3737, Jul. 2017.

[15] Y. Cao, Y. Zhang, Y. Cai, J. Zhang, and Z. Qian, "Wideband and high gain patch antenna loaded with mushroom-type metamaterial," in *Proc. Int. Conf. Microw. Millim. Wave Technol.*, May 2018, pp. 1–3.